

# Diffractive Higgs boson production at Tevatron and LHC: an experimental review

C. Royon\*

October 30, 2018

## Abstract

We discuss the different models of central diffractive production of the Higgs boson at the Tevatron and the LHC. We also describe how the models can be tested using diffractive production data being taken at the Tevatron. We finally discuss the advantages of using diffractive events to reconstruct the mass of the Higgs boson especially at the LHC.

## 1 Introduction and motivation

The discovery of the Higgs boson is one of the main goals of searches at the present and next hadronic colliders, the Tevatron and the LHC. The few Higgs boson candidates found at the end of LEP II [1] motivate the search for Higgs boson production for a Higgs mass in the 115-120 GeV region, specially at the Tevatron. Since this search will be quite difficult at Tevatron, it is important to find different ways to search for Higgs bosons. The LHC is clearly the golden accelerator to look for Higgs bosons. However, the domain at low masses ( $M_H < 160$  GeV) is the most difficult. In that mass domain, the Higgs boson decays mainly into  $b\bar{b}$ ,  $\tau^+\tau^-$  (for about 10% of the events) and into  $\gamma\gamma$  (for about 0.1% of the events). Because of the high background in the  $b\bar{b}$  or  $\tau^+\tau^-$  channels, only the  $\gamma\gamma$  one seems to be relevant in the standard case and needs quite high luminosity (about  $50 \text{ fb}^{-1}$  to get a  $5\sigma$  discovery) and a precise calibration of the calorimeter. It is thus important to find other ways of looking for Higgs bosons in the 115-160 GeV mass range, even at the LHC.

The models of diffractive production of jets, leptons, photons or Higgs bosons are given in Figs. 1, 2 and 3. In Fig. 1 and 2, we give the schematic production for the inclusive mechanism. As shown in Fig. 1, the diffractive Higgs boson cross section is computed by taking the quark and gluon densities in the pomeron from the H1 experiment at HERA [4, 6]. These densities are then convoluted with the hard subprocess, namely the Higgs boson production via a top loop. In the second set of models, see Fig. 2, we take the usual hadron-hadron cross section to produce the hard scattering (Higgs, dijets,  $\gamma\gamma$ ) and convolute it with the normalised parton densities inside the pomeron taken from the H1 experiment [5]. The third set of models [3] called exclusive is completely different since it does not assume the existence of a colorless object in the proton like the pomeron, and gives a perturbative calculation of the diffractive process using the gluon density in the proton (at the lowest order, the exchange of two gluons is assumed in order to get a colorless object). We will now discuss all these models in more detail, and give their

---

\*CEA/DSM/DAPNIA/SPP, F-91191 Gif-sur-Yvette Cedex, France, email royon@hep.saclay.cea.fr

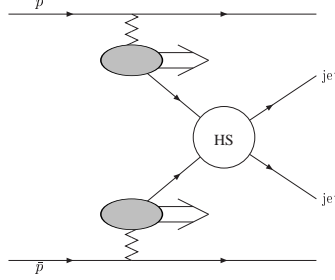


Figure 1: Diffractive jet production via the factorisable inclusive production mechanism. (Fig taken from Ref. [2]).

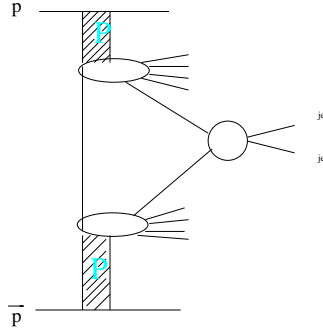


Figure 2: Diffractive jet production via the non factorisable inclusive production mechanism. (Fig taken from Ref. [5]).

predictions concerning the Higgs boson production cross section. We will also discuss how to test these models using Tevatron data.

## 2 Inclusive Higgs production

### 2.1 Factorisable inclusive Higgs production

The factorisable inclusive Higgs and dijet production cross sections have been presented in Ref. [2, 6]. In this model, the diffractive gluon density is taken from the H1 measurement [4] at HERA and is used to compute the diffractive dijet, diphoton or Higgs boson cross sections, by convoluting this parton density with the standard hard subprocess (diquark or Higgs boson production via a top loop). The cross sections obtained are given in Table 2.1 for the pomeron and reggeon contributions. We will discuss the assumptions of this model in the following. In this model, factorisation breaking between HERA and Tevatron is assumed to give a factor 0.1 in normalisation for the Higgs or dijet production cross sections

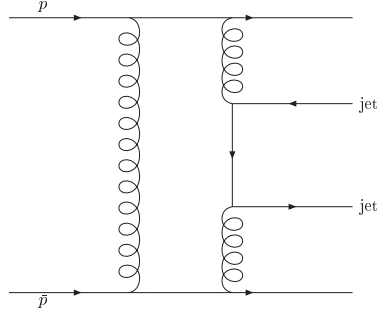


Figure 3: Diffractive jet boson production via the exclusive production mechanism. (Fig taken from Ref. [2]).

at the Tevatron. Since this number is not known at LHC energies, no factor has been applied for the Higgs boson production cross sections at the LHC. We note that the cross section is very low at the Tevatron and quite high at the LHC, provided the survival gap probability is not too small.

## 2.2 Non factorisable inclusive Higgs production

The non factorisable inclusive Higgs, dijet, diphoton and dilepton production cross sections have been presented in Ref. [5]. The main difference with the previous model is that the usual soft hadron-hadron cross section is assumed to produce the hard scattering, and this cross section is then convoluted with the partonic densities in the pomeron taken from the H1 experiment (see the third item of Ref. [5] to get a detailed description of the theoretical framework of this model). A soft gluon is present between the two protons which implies in this model a natural factorisation breaking between the Tevatron and HERA. The pomeron intercept is thus the soft one in this model ( $\epsilon = 0.08$ ) [7] whereas a hard value of the pomeron intercept is used in the previous model ( $\epsilon = 0.2$ ).

We will also discuss in the following the assumption of taking the quark and gluon densities from HERA in this model and to apply them to the Tevatron and the LHC. This model has been interfaced with PYTHIA [8] for hadronisation. The generator has also been interfaced to a fast simulation of the

| Process                                    | Pomeron | Total | Total*GSP | GSP |
|--|---------|-------|-----------|-----|
| $H \rightarrow bb$ , $m_H = 115$ GeV, Tev. | 0.19    | 0.21  | 0.02      | 0.1 |
| $H \rightarrow WW$ , $m_H = 160$ GeV, Tev. | 0.003   | 0.003 | 0.0003    | 0.1 |
| $H \rightarrow bb$ , $m_H = 115$ GeV, LHC  | 176     | 276   | 276       | 1.  |
| $H \rightarrow WW$ , $m_H = 160$ GeV, LHC  | 97      | 133   | 133       | 1.  |

Table 1: Higgs boson production cross section in fb at the Tevatron and the LHC for Higgs masses between 115 and 160 GeV for the *inclusive factorisable* models. The gap survival (GSP) probability used in this model is also given. At the LHC, the GSP is taken to be 1.0 since it is not known and all results should be multiplied by its value (it should be however less than 0.1) (see Ref. [6] for more detail).

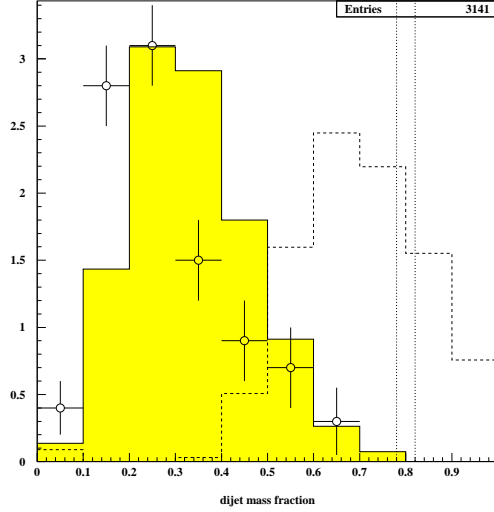


Figure 4: Observed dijet mass fraction (CDF Run I), compared to the non-factorisable pomeron based model prediction (full line), using the Pomeron structure functions from H1. We also give the comparison with exclusive models before (dotted line) or after (dashed line) simulation of the detector.

DØ and CDF detectors, which allowed to scale the prediction to the CDF Run I measurement [9], namely  $\sigma \sim 43.6 \pm 4.4$  (stat.)  $\pm 21.6$  (syst.) nb when the antiproton is tagged in the roman pot detectors in the following kinematical domain in  $\xi$  and  $t$  of the proton and the antiproton ( $0.035 \leq \xi_{\bar{p}} \leq 0.095$ ,  $|t| < 1$  GeV<sup>2</sup>,  $0.01 \leq \xi_p \leq 0.03$ ).

The prediction of this model has also been compared with the dijet mass fraction measured by the CDF collaboration [9]. The results are shown in Fig. 4. The black points correspond to the CDF measurements and they are compared with three different curves: the dotted line gives the prediction at the generator level without any structure function for the pomeron (bare cross section), the dashed line gives the same result after simulation of the detector and again no structure assumed for the pomeron and the full line gives the result of the detector simulation and the effect of taking the quark and gluon densities in the pomeron from the H1 experiment. We note that we need both a pomeron made of quarks and gluons, the parton densities being taken from HERA, and a simulation of the CDF detector to describe this measurement. Furthermore, if we assume a different structure function of the pomeron than the one from H1, namely the same kind of structure function as in the proton (we took the GRV [10] parametrisation to do this test), we get a bad description of the dijet mass fraction (see Fig. 5).

The results concerning the Higgs boson cross sections at the Tevatron and the LHC are given in Table 2.2 and in Fig. 6. We note that the cross sections at the Tevatron are quite low like in the previous model and quite large at the LHC. In this model, there is no need to apply a survival gap probability since the cross section has been rescaled to the CDF measurement. It is however important to note that the scaling factor might be different at the LHC while the same factor between the Tevatron and the LHC has been assumed.

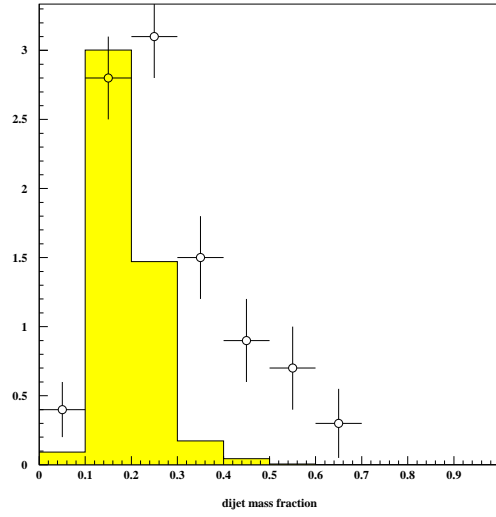


Figure 5: Dijet mass fraction obtained using the gluon structure function from the proton.

| $M_{Higgs}$ | Total | $bb$ | $\tau\tau$ | $W^+W^-$ |
|-------------|-------|------|------------|----------|
| 120, Tev.   | 1.3   | 0.9  | 0.1        | 0.1      |
| 140, Tev.   | 0.3   | 0.1  | 0.0        | 0.2      |
| 120, LHC    | 15.9  | 11.4 | 1.0        | 1.8      |
| 140, LHC    | 13.8  | 5.4  | 0.5        | 6.2      |
| 160, LHC    | 12.3  | 0.6  | 0.1        | 10.9     |

Table 2: Higgs boson production cross section in fb at the Tevatron and the LHC for different Higgs masses for the inclusive non factorisable models. (see Ref. [5] for more detail).

## 2.3 Factorisation breaking between HERA and Tevatron?

As we mentioned in the previous sections, one assumption concerning both models was to take the gluon and quark densities in the pomeron measured at HERA, in the H1 experiment [4] to compute the Higgs boson production cross section. In Fig. 7, we show the recent determination of the gluon density inside the pomeron made by the H1 collaboration [12] using the most recent diffractive structure function data (full red line). The curve is compared to the CDF gluon density determination [12] (black points). We notice that both curves show largely different normalisations but similar shapes. This justifies a priori to take a constant normalisation factor difference between HERA and the Tevatron, while keeping the same gluon density. More precise measurements at the Tevatron being performed using the CDF roman pot detectors or the new implemented Forward Proton Detector from DØ [13] will be needed and available soon to test further this hypothesis.

It is clear however that we need some more studies concerning how the normalisation factors vary as a function of energy to transfer the results from the Tevatron to the LHC. One approach to perform this is to study experimentally the price to pay to get one gap (or one tag in the roman pot detectors) versus two gaps, since we know already that the percentage of events showing two gaps is larger than the squared percentage of events showing only one gap [15].

## 2.4 SUSY Higgs production cross section enhancement

Of particular interest are the SUSY based models where mass of the Higgs boson is expected to be small. In this section, we will discuss briefly the enhancement in Higgs boson production cross sections valid for all models (exclusive or inclusive) within supersymmetric models. At high  $\tan\beta$ , not only top quark loops have to be considered but also bottom quark loops [11]. The results concerning the Higgs  $h$  boson cross section are given in Fig 8. The upper plot gives the enhancement factor as a function of the Higgs mass for  $\tan\beta=30$  and the top and sbottom squark masses of 300 GeV in the case where stops are not degenerate (maximal mixing). We note an enhancement of a factor 10 for a Higgs mass of 105 GeV for instance. The bottom plot show the distribution as a function of  $\tan\beta$  for a Higgs mass of 100 GeV and we note an enhancement of the cross section of a factor 40 for  $\tan\beta \sim 50$ . In this domain the Higgs boson decays mainly into  $b\bar{b}$  (the branching ratio into  $\gamma\gamma$  is much smaller than in the case of the standard model), and it is worth looking for it in the diffractive channel where  $H \rightarrow b\bar{b}$  can be used. The standard non-diffractive search for Higgs bosons in this mass region does not benefit from the increase in cross section since the branching ratio into  $\gamma\gamma$  decreases at the same time.

## 2.5 Tests of the models at the Tevatron and differences between the factorisable and non factorisable models

Even if the diffractive Higgs boson production cross sections are too low at the Tevatron, important tests of the models concerning dijet, diphoton and dilepton production can be done, which will allow to make more precise predictions for the LHC. All models give predictions for these cross sections and we give in Figs 9, 10, 11, 12 [5] the predictions for the non factorisable inclusive model. All these measurements will be performed soon by the CDF and DØ experiments and will perform good tests of the model [14].

It is also important to be able to distinguish between the two inclusive models, the factorisable and the non factorisable one. As we mentioned before, one of the main differences between both models is the value of the pomeron intercept which is the soft one ( $\epsilon = 0.08$ ) in the non factorisable model, and the hard one measured at HERA ( $\epsilon = 0.2$ ) in the case of the factorisable one. Another difference is due to

the presence of a soft gluon between both pomerons in the case of non-factorisable models (see Fig. 2). In Fig. 13 is given the differential dijet cross-sections for different values of  $\epsilon$ , compared to a reference taken at  $\epsilon = 0.08$ . All cross-sections are normalised to the same value. We note that the measurement of  $\epsilon$  can be performed using the measurement of the differential dijet mass cross section. Fig. 14 also shows that the measurement of the slope of the dijet mass cross section may lead to a measurement of  $\epsilon$  even if this measurement is not easy. Such a measurement will allow to distinguish between the factorisable and non factorisable models and will perform a direct measurement of the pomeron intercept at the Tevatron.

## 2.6 Roman pot detectors at the Tevatron and the LHC: where to put them?

In this section, we will discuss the optimal positions to detect Higgs bosons at the Tevatron or the LHC. In Fig. 15, we give the  $\xi$  vs  $t$  distributions for diffractive Higgs boson production. The size of the squares is proportional to the cross section given by the non factorisable model. The upper plot give the  $\xi$  vs  $t$  distribution at the Tevatron for a Higgs mass of 120 GeV, the lower left plot for a Higgs mass of 120 GeV at the LHC, and the lower right plot for a Higgs mass of 800 GeV at the LHC (which is basically the same plot as the upper one, the difference being due only to the difference of beam energies). We notice that we need a good acceptance at high  $t$  ( $|t| > 0.2$ ) and high  $\xi$  ( $\xi > 0.05$ ) at the Tevatron, and at high  $t$  ( $|t| > 0.2$ ) and low  $\xi$  ( $\xi < 0.02$ ) at the LHC.

The CMS [16] and Totem collaborations proposed to install a few sets of roman pot detectors showing the following acceptances:

- (1): 140-180 meter pots (standard TOTEM)  $|t| < 1.5 \text{ GeV}^2$ ,  $\xi > 0.02$
- (2): 240 meter pots (addition in warm section), and TOTEM  $|t| < 2 \text{ GeV}^2$ ,  $\xi > 0.01$
- (3): 425 meter pots (cold section)  $|t| < 2 \text{ GeV}^2$ ,  $0.002 < \xi < 0.02$
- (4): All pots  $|t| < 2 \text{ GeV}^2$ ,  $\xi > 0.002$

We notice that we need to have roman pots or microstations [17] in the cold region of the LHC if we want to have a good acceptance for diffractive Higgs production at the LHC. In the following, we will assume that the CMS Collaboration has all pots (case number 4) when we discuss the advantage of reconstructing the Higgs mass using roman pot detectors or microstations [14].

## 3 Exclusive diffractive Higgs boson production

In this kind of models [3] a direct perturbative calculation of the diagram (see 1) is performed using the gluon density in the proton. This leads to very clean events where the protons are scattered at very small angle in the beam pipe (and can be tagged in roman pot detectors or microstations) and the Higgs boson which decays centrally in the main detector, and nothing else. The problem is that one needs to suppress totally QCD radiation. The price to pay to get this kind of events is an exponential Sudakov form factor to suppress QCD radiation which leads to a low cross section. One may wonder if these events exist (no soft gluon can be emitted after interaction), which can be tested at the Tevatron [15]. The diffractive Higgs boson cross section for this process is given in Table 3. We note that the cross sections are extremely small for the Tevatron and quite large enough for the LHC provided that the gap survival probability is not too small.

| $M_{Higgs}$ | Tevatron | LHC  |
|-------------|----------|------|
| 120         | 0.03     | 1.4  |
| 140         | 0.02     | 0.9  |
| 160         | 0.008    | 0.55 |

Table 3: Higgs boson production cross section in fb at the Tevatron and the LHC for different Higgs boson masses for the exclusive models. (see Ref. [3] for more detail). (Note that no gap survival probability has been applied for the LHC).

At the Tevatron, it is important to check if the exclusive events exist or not and to measure their production cross section since they have never been observed yet. These events would be the ideal ones for the LHC. So far, the CDF collaboration looked at these events in the dijet channel and put a limit of 3.7 nb on their production cross section [15]. The difficulty is to distinguish these exclusive events from *quasi-exclusive* events produced in inclusive events. Namely, it is possible to produce events inclusively where most of the energy in the pomeron is used to produce dijets, diphotons, dileptons or Higgs bosons, or in other words, where pomeron remnants show very little energies. These “quasi-exclusive” events will be very similar to the exclusive ones and it is thus important to see how one can distinguish between them, and see if exclusive events exist or not. One way to distinguish between them would be to measure the ratio of the diffractive diphoton to dilepton cross sections at the Tevatron. In Fig. 16, we give the diphoton to dilepton cross-section ratio, as a function of the mass fraction (the diphoton or dilepton mass divided by the total diffractive mass). In inclusive models, this ratio is determined by the quark and gluon distributions inside the Pomeron, and the presence of the Z pole in the dilepton cross-section. In exclusive models, it is only possible to produce diphoton diffractively but no dilepton. The diphoton cross section obtained for a mass fraction higher than 0.85-0.9 is of the order of 2 fb for both the exclusive and inclusive cross sections, and the ratio of the diphoton to dilepton cross section measured at the Tevatron is expected to show an enhancement and a change of slope as a function of the diphoton/dilepton mass if exclusive events exist. This will be a very clean test of the existence of exclusive events. Another possible test will be to measure the  $\chi_b$  or  $\chi_c$  central diffractive production cross section.

## 4 Soft colour interaction models

In this section, we will discuss a completely different model based on soft interaction in the final state which happen after the hard interaction at a longer time scale. Two versions of a model have been designed to describe diffractive physics as soft color rescattering over a hard subprocess [18], namely SCI (Soft Color Interaction) and GAL (General Area Law). These models do not imply the existence of colourless objects like the pomeron since diffraction is explained by soft interactions in the final state. Color exchanges occur in the final state, potentially stopping color flow between the remnants of the incoming hadrons and the central system, leading to diffractive event topologies. They are implemented as a transition between the hard interaction and hadronization, and therefore fit naturally in Monte-Carlo programs such as PYTHIA [8].

Their prediction concerning diffractive Higgs production are given in Table 4. Very low cross sections are obtained at the Tevatron and quite low cross sections at the LHC (even if they are high enough to be measured at the LHC because of the high value of the luminosity). The disadvantage of this model is that it does not describe perfectly final states where a tagged proton is detected in the final state,



| $M_{Higgs}$ | Tevatron                       | LHC         |
|-------------|--------------------------------|-------------|
| 115         | $1.2\text{-}2.4 \cdot 10^{-4}$ | 0.162-0.189 |

Table 4: Higgs boson production cross section in fb at the Tevatron and the LHC for soft colour interaction models. (see Ref. [18] for more detail).

especially at HERA.

## 5 Higgs mass reconstruction using diffractive events

### 5.1 Higgs mass reconstruction in the case of exclusive events

Exclusive Higgs events are diffractive events where all the energy (basically all diffractive mass) is used to produce the Higgs boson. Kinematically, it is very easy to reconstruct the Higgs mass if one is able to measure the  $\xi$  of both scattered protons detected in roman pot detectors [19]:  $M_{Higgs} = \sqrt{\xi_{p1}\xi_{p2}S}$ . The mass reconstructed using roman pot detectors with a resolution in  $\xi$  of 0.2% , and in  $t$  of 10%  $\sqrt{t}$  is given in Fig. 17. We note that these events allow to get a perfect Higgs mass reconstruction with a resolution better than 1%. This resolution allows a very good signal over background separation.

The experimental difficulty is to trigger on these events. Since the microstations or roman pot detectors are located far away from the main experiments (Atlas or CMS), the trigger informations from these detectors will only arrive at the second level. At the first level, it is needed to trigger on energy deposited in the calorimeters requiring for instance the presence of the Higgs decay products as well as little energy in the forward region. At the second level, the trigger can require a matching between masses calculated using the calorimeter or the microstation information. Of course, a detailed simulation is needed to make more precise statements [14].

### 5.2 Higgs mass reconstruction in the case of inclusive events

In the case of inclusive events, the previous method to reconstruct the mass of the Higgs boson will not work so nicely since the total energy is used not only to produce the Higgs boson, but also lost in the pomeron remnants. The natural idea is to cut on the energy of the pomeron remnants to be able to get quasi-exclusive events where not much of the available energy is lost in pomeron remnants. The CMS collaboration [16] will be able to tag particles up to a rapidity of 7.5. In Fig. 18, we give the resolution obtained on the Higgs mass reconstruction if one is able to cut on the energy of the pomeron remnant (in these plots, we assume that we are able to tag the remnants up to a rapidity of 7.5, and the resolution of these detectors to be  $100\%/\sqrt{E}$ ). The resolution of the Higgs mass is found to be about 2.1, 4.0, 4.6 and 6.6 GeV if one requires the remnant energies below a rapidity of 7.5 to be respectively less than 20, 50, 100 and 500 GeV at the LHC. Of course this method will work only during the first three years at the LHC when the luminosity will be low because of pile-up events. Of special interest are the cases when the Higgs boson decays into  $\tau$  because of the low diffractive background.

| Process  | (1)  | (2)         | (3)  | (4)        |
|--|------|-------------|------|------------|
| $\gamma\gamma$ , Tev, $E_T > 12\text{GeV}$ , $\eta < 2$  | 71.  | 128. (27.)  | -    | $\sim 20.$ |
| $\gamma\gamma$ , Tev, $E_T > 12\text{GeV}$ , $\eta < 1$  | 9.   | 8. (2.)     | -    | -          |
| $\gamma\gamma$ , LHC, $E_T > 50\text{GeV}$ , $\eta < 2$  | 1.5  | -           | -    | 0.1        |
| $\gamma\gamma$ , LHC, $E_T > 120\text{GeV}$ , $\eta < 5$ | 19.  | -           | 0.12 | -          |
| Higgs, 115 GeV, Tev                                      | 1.7  | 0.029-0.092 | 0.2  | 0.00012    |
| Higgs, 115 GeV, LHC                                      | 169. | 379.-486.   | 2.8  | 0.19       |
| Higgs, 160 GeV, LHC                                      | 123. | 145.        | 1.0  | -          |

Table 5: Diphoton and Higgs boson cross sections (fb) for the different models discussed: 1: inclusive non factorisable models, 2: inclusive factorisable models (note that no GSP is used for the LHC), 3: exclusive models, 4: models of soft colour interaction

## 6 Conclusion

In this short review, we have discussed the different models of production of diffractive Higgs bosons. We can distinguish between three different sets of models: inclusive, exclusive or soft interaction. All models (even the soft colour ones) show low cross sections at the Tevatron and high enough cross sections at the LHC. A noticeable enhancement of the production cross section can be obtained in SUSY models with high values of  $\tan\beta$ . It is thus very important to test these models using Tevatron data being taken now, to get more precise cross section predictions for the LHC. The Higgs mass reconstruction is greatly improved by using roman pot detectors or microstations at the LHC, which enhances the signal to background ratios and allows to use the  $b\bar{b}$  and the  $\tau\tau$  Higgs decay channels for exclusive [3] or quasi-exclusive events [14].

To summarise, we give in Table 6 the cross sections given by the four different models described in this review both for the Higgs and diphoton predictions when they are available.

## Acknowledgments

Most of these results come from a fruitful collaboration with Maarten Boonekamp, Robi Peschanski and Albert de Roeck. I also wish to thank Mike Albrow, Valery Khoze, Stéphane Lavignac, Risto Orava, and Laurent Schoeffel for useful discussions.

## References

- [1] LEP Higgs working group, preprint CERN-EP/2003-011, submitted to *Phys. Lett. B*.
- [2] R. B. Appleby, J. R. Forshaw, *Phys. Lett. B* **541**(2002) 108.
- [3] V. A. Khoze, A. D. Martin, M. G. Ryskin, *Eur.Phys.J. C* **24** (2002) 581, *Eur.Phys.J. C* **23** (2002) 311, *Eur.Phys.J. C* **25** (2002) 391.
- [4] H1 Collab., C. Adloff et al., *Z. Phys. C* **76** (1997) 613.

- [5] M. Boonekamp, R. Peschanski and C. Royon, *Phys. Rev. Lett.* **87** (2001) 251806, M. Boonekamp, A. De Roeck, R. Peschanski and C. Royon, hep-ph/0205332, *Phys. Lett.* **B550** (2002) 93, M. Boonekamp, R. Peschanski and C. Royon, hep-ph/0301244, *Nucl. Phys.* **B**, to appear.
- [6] B. Cox, J. Forshaw, B. Heinemann, *Phys. Lett.* **B540** (2002) 263
- [7] A. Bialas and P. V. Landshoff, *Phys. Lett.* **B256** (1990) 540; A. Bialas and W. Szeremeta, *Phys. Lett.* **B296** (1992) 191; A. Bialas and R. Janik, *Zeit. für. Phys.* **C62** (1994) 487.
- [8] T. Sjostrand, P. Eden, C. Friberg, L. Lonnblad, G. Miu, S. Mrenna, E. Norrbin, *Comput. Phys. Commun.* **135**(2001) 238.
- [9] CDF Collab., T. Affolder et al., *Phys. Rev. Lett.* **85** (2000) 5043.
- [10] M. Glück, E. Reya, A. Vogt, *Z. Phys.* **C41** (1988) 667, **C48** (1990) 471, **C53** (1992) 651, **C67** (1995) 433, *Eur. Phys. J.* **C5** (1998) 461.
- [11] M. Boonekamp, P. Demine, S. Lavignac, R. Peschanski, C. Royon, in preparation.
- [12] P. Laycock, *talk given at 10th Intl. Workshop on Deep Inelastic Scattering (DIS 2002), Cracow, May 2002*, *Acta Phys. Polonica* **B33, N.11** (2002) 3413; F.P. Schilling *idem*, hep-ex/0209001, *Acta Phys. Polonica* **B33, N.11** (2002) 3419; P.R. Newman, *Talk at low-x Meeting, Antwerpen, September 2002*.
- [13] *Proposal for a Forward Proton Detector at D0*, D0 Collab. (1997), Proposal P-900 to Fermilab PAC.
- [14] J.-L. Agram, M. Boonekamp, R. Peschanski, C. Royon, in preparation.
- [15] CDF Coll., *Phys. Rev. Lett.* **85** (2000) 4215, D. Goulianos, *Talk at the low-x Meeting, Nafplio, June 2003*.
- [16] CMS Collab., Technical Design Report (1997), TOTEM Collab., Technical Design Report, preprint CERN/LHCC 99-7.
- [17] R. Orava, *talk at LISHEP02, Rio de Janeiro, February 2002*.
- [18] R. Enberg, G. Ingelman, A. Kissavos, N. Timneanu, *Phys. Rev. Lett.* **89** (2002) 081801
- [19] M. G. Albrow and A. Rostovtsev, hep-ph/0009336.

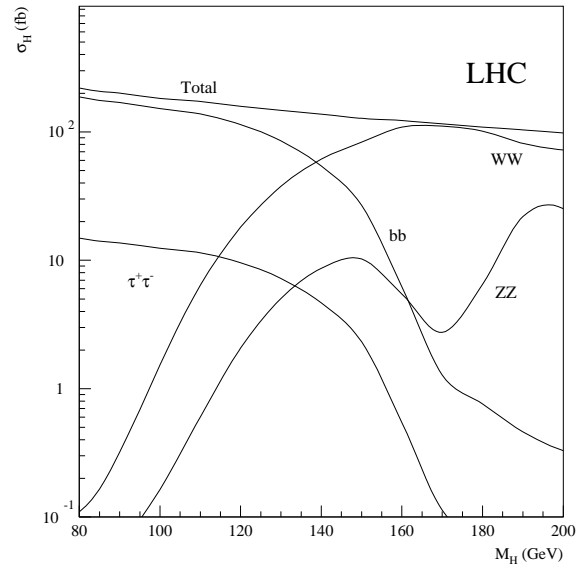


Figure 6: Higgs boson production cross-section at the LHC. Various decay channels are plotted as a function of the mass of the Higgs boson .

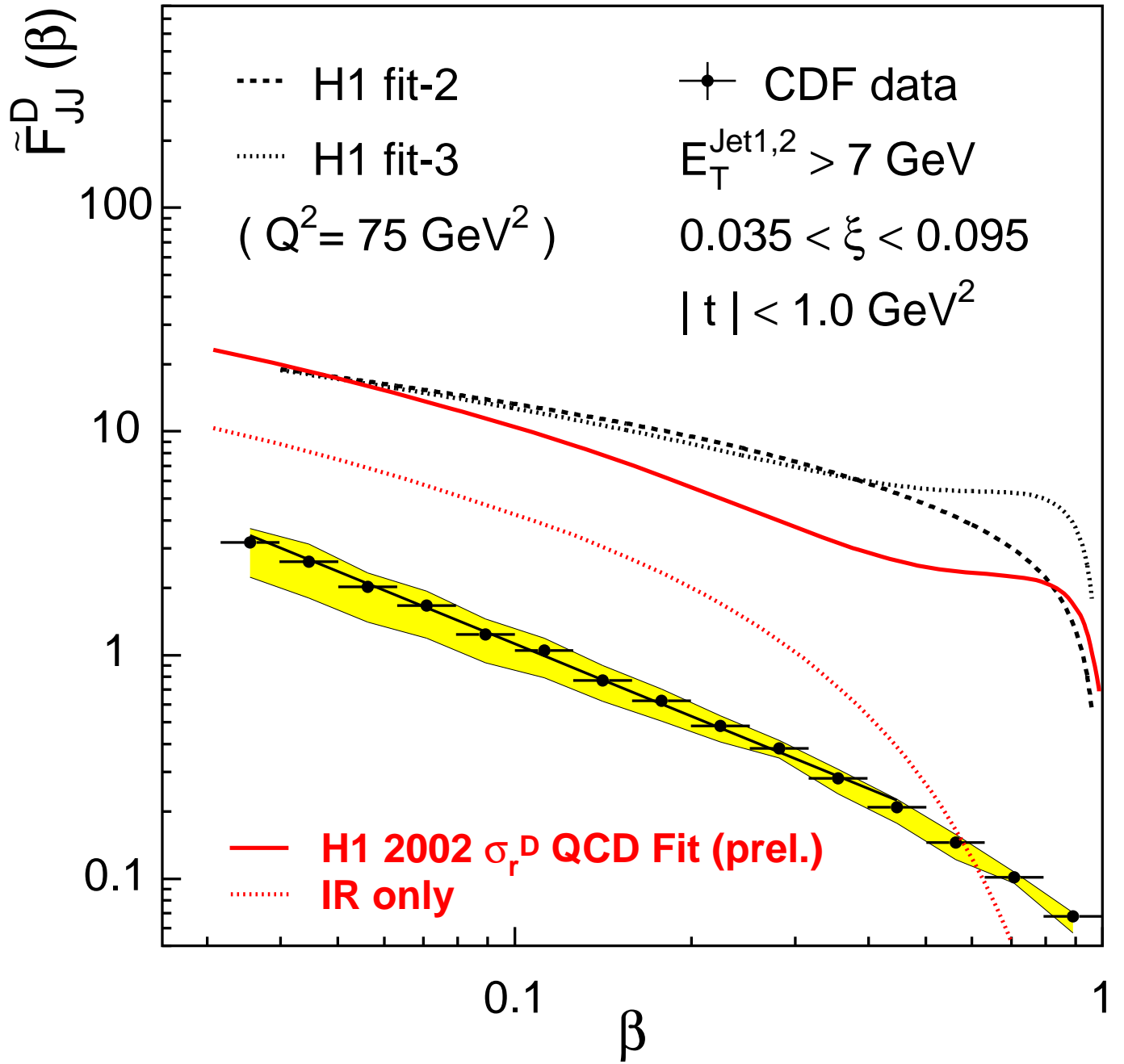


Figure 7: Results of the new determination of the gluon density in the pomeron from the H1 collaboration (full line) compared with the CDF measurement (see Ref. [12] for more detail). (The lower dotted line represents the reggeon contribution, and the dashed and upper dotted lines the results of a fit using only 1994 data from the H1 collaboration.)

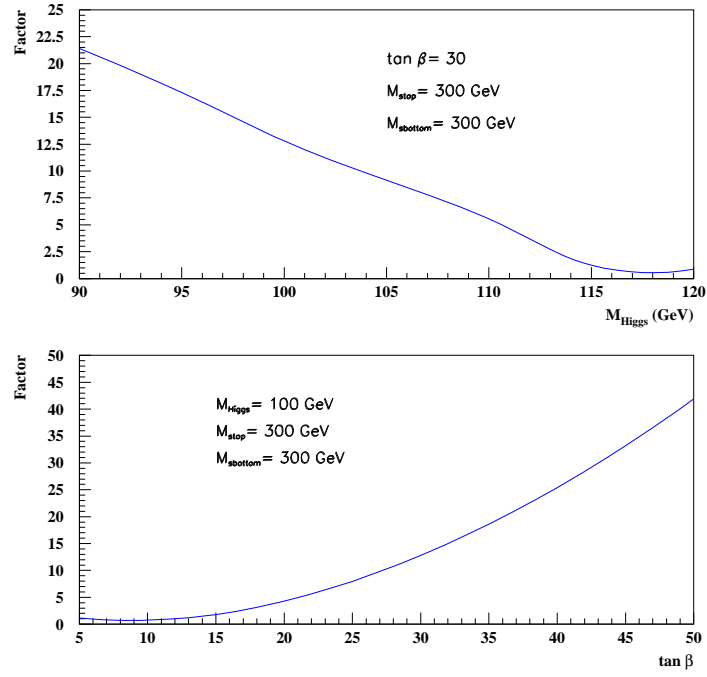


Figure 8: Enhancement factor concerning Higgs boson production cross section in a SUSY scenario compared to the standard model case as a function of the Higgs mass and the  $\tan \beta$  parameter.

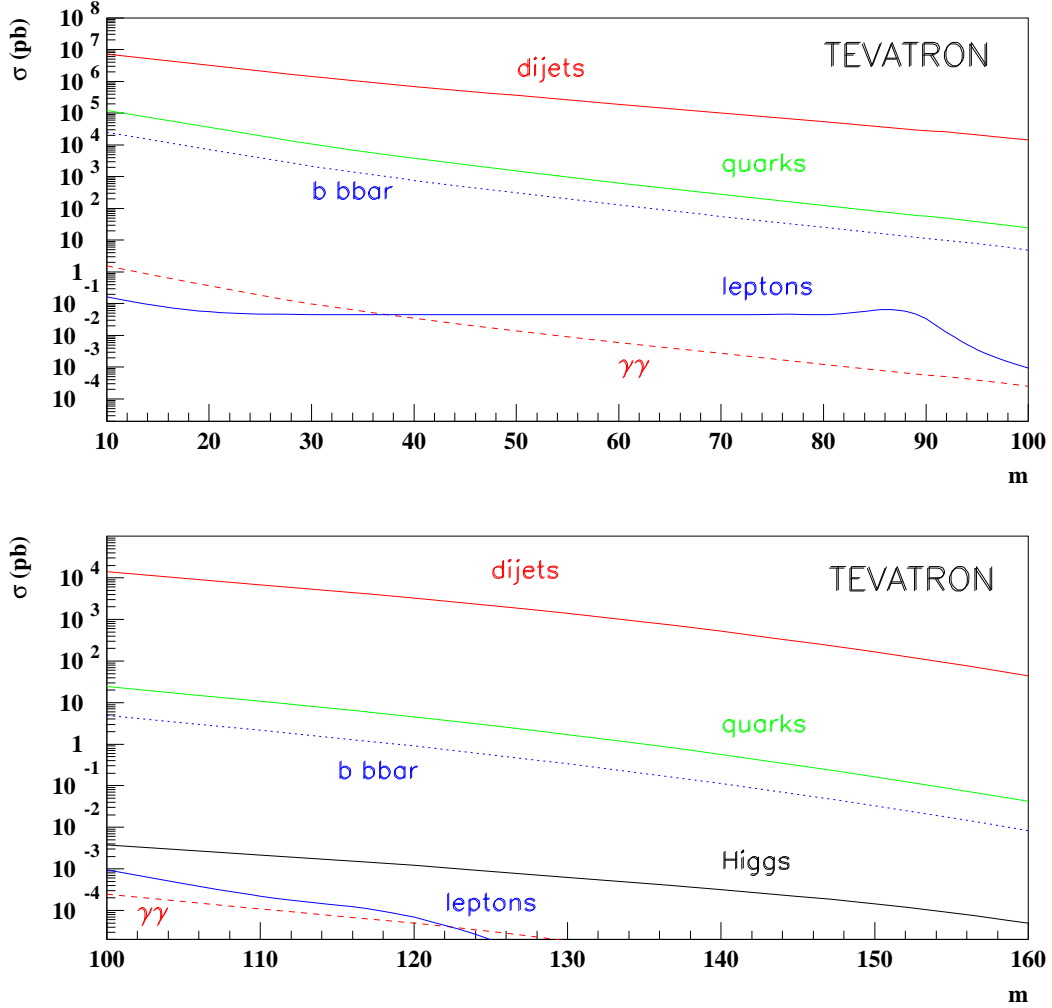


Figure 9: Dijet, diquark,  $b\bar{b}$ , dilepton, and diphoton cross-sections (pb) at the Tevatron. The cross-sections are given for a mass  $m$  above the value on the abscissa, for two different mass ranges. For comparison, we also display the Higgs boson cross-section for  $M_{Higgs} = m$ .

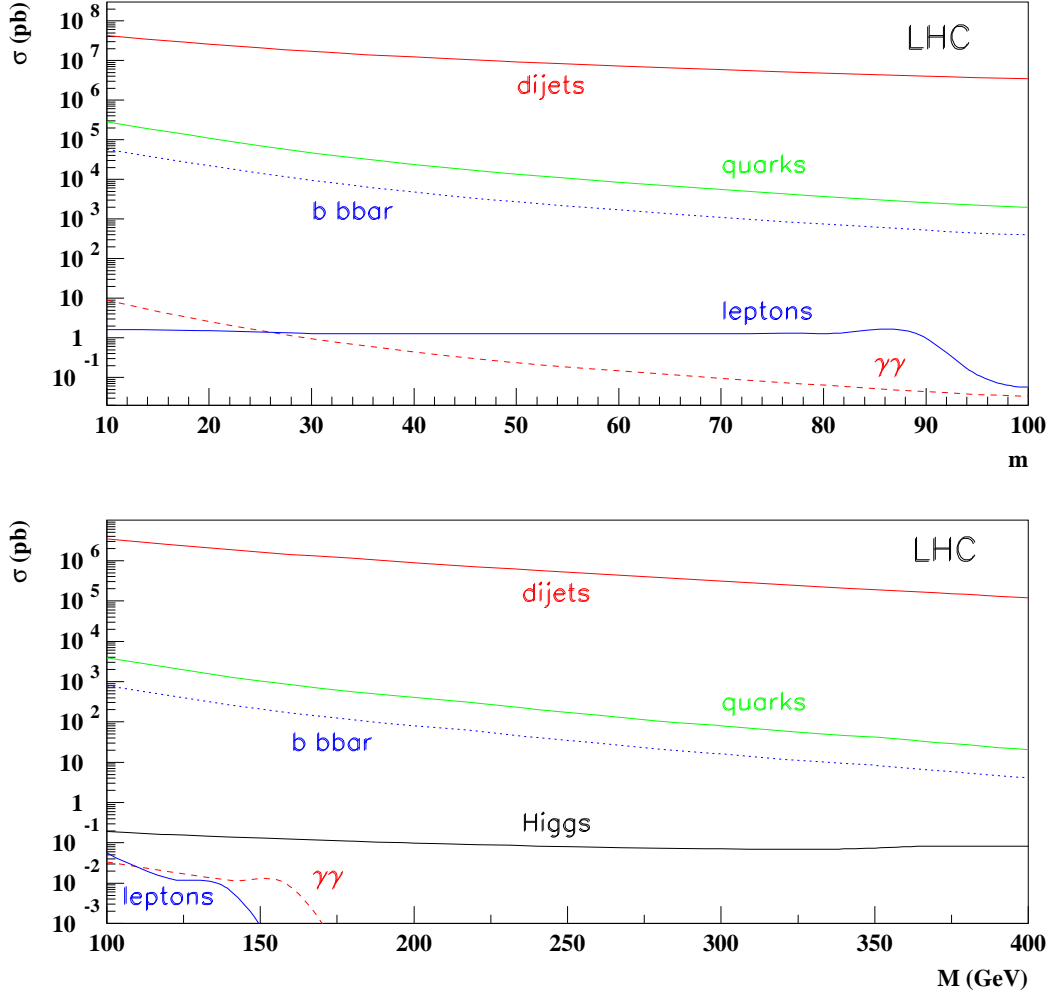


Figure 10: Dijet, diquark,  $b\bar{b}$ , dilepton, and diphoton cross-sections (pb) at the LHC. The cross-sections are given for a mass  $m$  above the value on the abscissa, for two different mass ranges. For comparison, we also display the Higgs boson cross-section for  $M_{Higgs} = m$ .



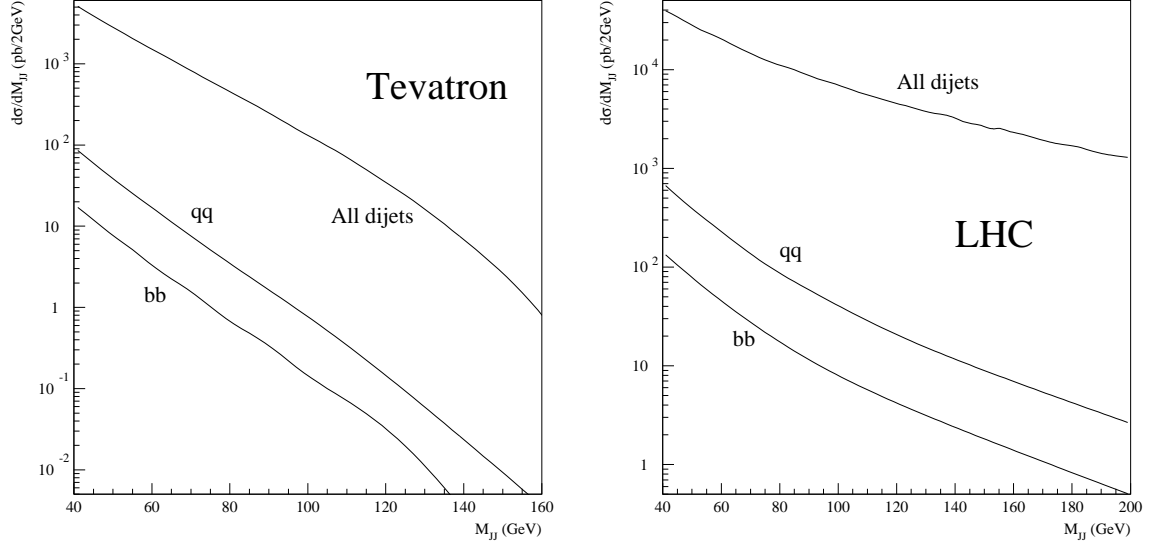


Figure 11: Differential dijet production cross-section (pb) at the Tevatron and the LHC. The transverse energy of the central jets satisfies  $E_T > 10$  GeV, and their rapidity is limited to  $|y| < 4$ .

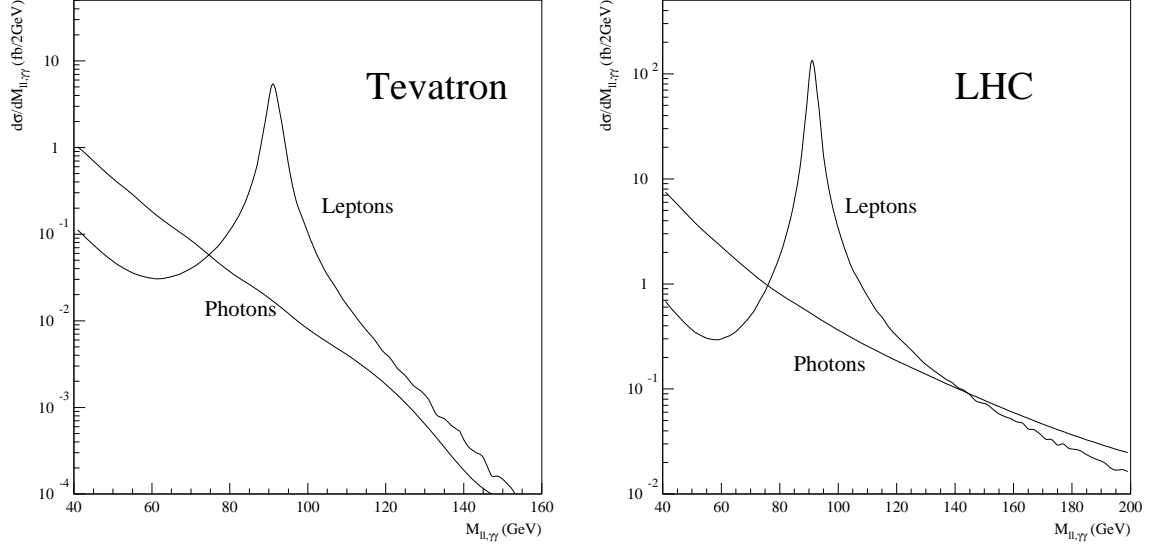


Figure 12: Differential diphoton and dilepton production cross-sections (fb) at the Tevatron and the LHC. The dilepton cross-section corresponds to a single lepton flavour. The transverse energy of the central particles satisfies  $E_T > 10$  GeV, and their rapidity is limited to  $|y| < 4$ .

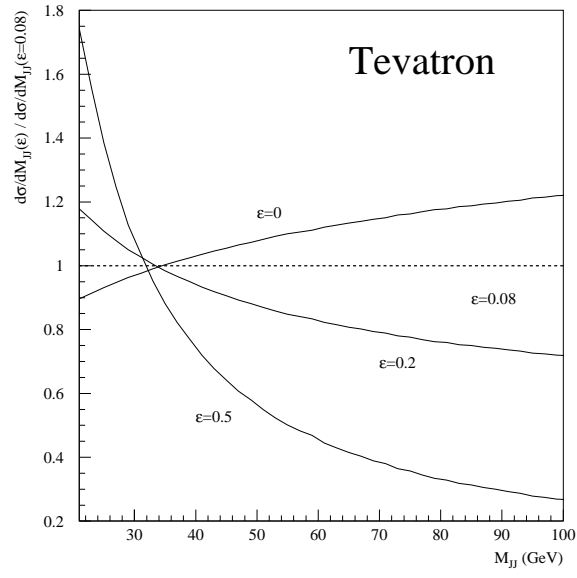


Figure 13: Differential dijet cross-sections for different values of  $\epsilon$ , compared to a reference taken at  $\epsilon = 0.08$ . All cross-sections are normalised to the same value. The values  $\epsilon = 0.08, 0.2$  and  $0.5$  correspond, respectively, to the soft, hard (measurement at HERA), and hard BFKL pomeron intercepts.

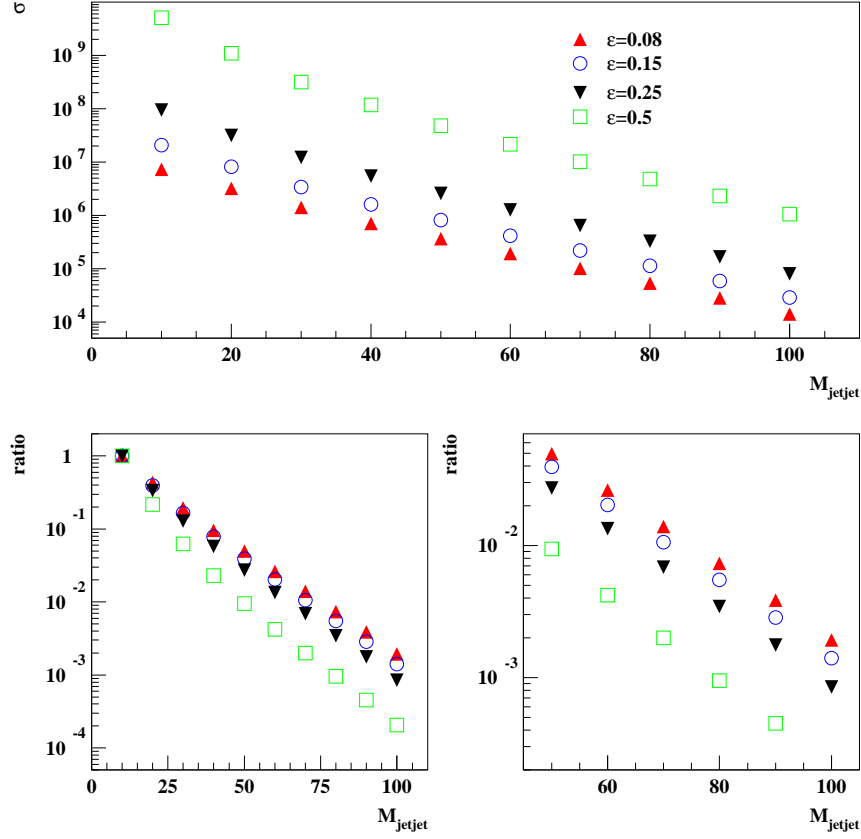


Figure 14: Variation of the dijet cross section for different values of  $\epsilon$  as a function of the dijet mass bin. The upper plot gives the different dijet cross sections at Tevatron energies. The lower plots show the same results when we put arbitrarily all cross section at 1.0 in the first dijet mass bin to show the differences in slope.

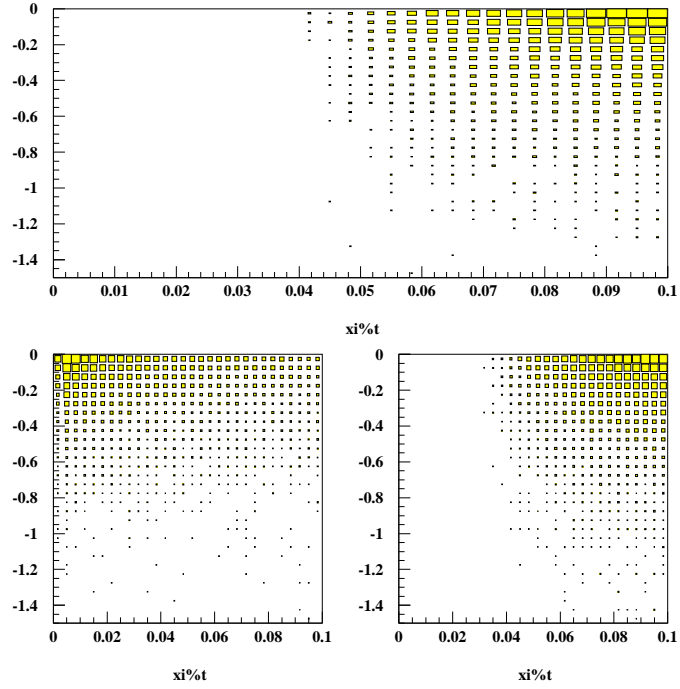


Figure 15:  $\xi$  vs  $t$  distributions for diffractive Higgs boson production. The size of the squares is proportional to the cross section given by the non factorisable model. The upper plot give the  $\xi$  vs  $t$  distribution at the Tevatron for a Higgs mass of 120 GeV, the lower left plot for a Higgs mass of 120 GeV at the LHC, and the lower right plot for a Higgs mass of 800 GeV at the LHC.

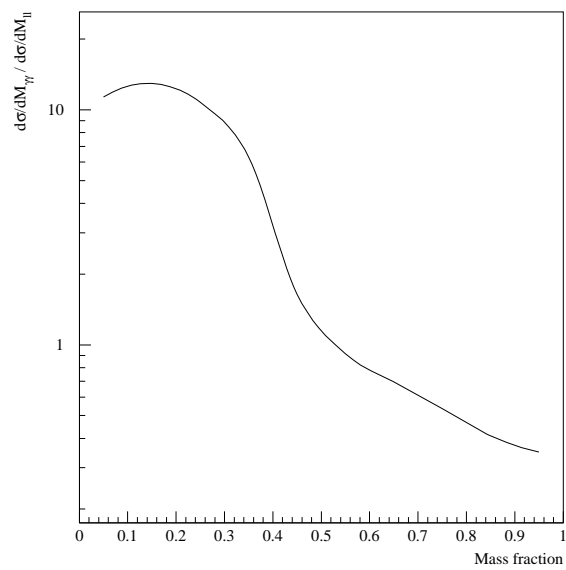


Figure 16: Diphoton to dilepton cross-section ratio, as a function of the mass fraction.

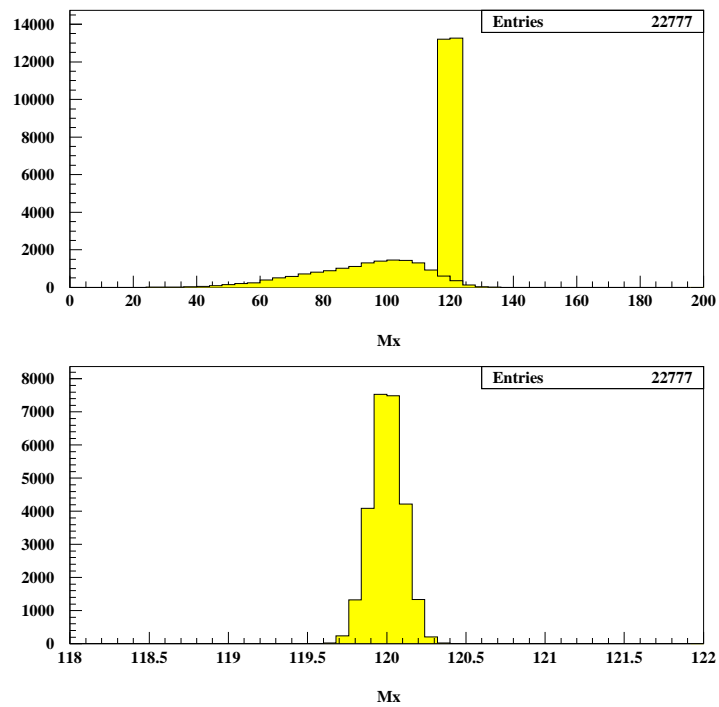


Figure 17: Higgs mass reconstruction for exclusive events using roman pot detectors.

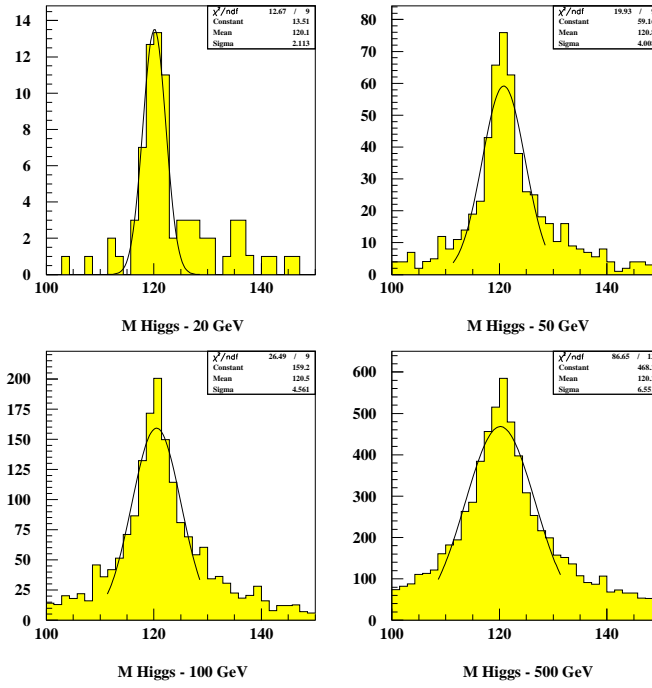


Figure 18: Higgs mass reconstruction for inclusive events using roman pot detectors, and central detectors up to a rapidity of 7.5 for a Higgs mass of 120 GeV at the LHC.